

Nickel Nanoparticles Modified Gold Electrode as Electrochemical Dopamine Sensor

A. A. AGALE¹, S. T. GAIKWAD², A. S. RAJBHOJ³

Department of Chemistry, Dr. Babasaheb Ambedkar Marathwada University Aurangabad, 431004, (MS) India.

*Corresponding Author Email: ashwiniagale2012@gmail.com

Abstract

A voltammetric sensor was developed for detection of dopamine by using cyclic voltammetry (CV). The sensing platform was nickel nanoparticles modified gold electrode (Ni-AuE). Nickel nanoparticles were synthesized by electrochemical reduction method, using TOAB as stabilizer. XRD, SEM-EDS and TEM results showed that NiNPs were highly porous, nanocrystalline. The Ni-AuE modified electrode observed reversible behavior with ferricyanide system which had about 1.80 times more surface area and exhibited higher currents for dopamine oxidation compared to bare AuE. These results indicate that Ni-AuE exhibited good platform and could be used for voltammetric determination of dopamine. DA signal were well resolved using DPV techniques compared to CV techniques, with DPV giving the best peak separation.

Keywords: Electrochemical cell, TOAB, Nickel oxide nanoparticles, CV, DPV etc.

INTRODUCTION

Dopamine (DA) a biogenic catecholamine, is an important neurotransmitter of the central nervous systems [1,2]. DA is a ubiquitous neurotransmitter (NTM) in mammalian brain tissues that plays an important physiological role in the functioning of central nervous, renal, hormonal and cardiovascular systems as an extra cellular chemical messenger endocrine cardiovascular and cognitive functions, as well as emotional processes in human metabolism [3,4]. Normal level of DA in brain allows usual freedom of movement whereas low DA may cause neurological disorders such as Schizophrenia and Parkinson's disease [5,6], excess DA in brain often cause pleasurable, rewarding feelings, and sometimes even euphoria [7]. In recent years, various methods for determination of DA have been employed, such as electrochemistry [8,12], capillary electrophoresis [13], high performance liquid chromatography [14] and fluorimetry [15]. However, the electrochemical measurement of neurotransmitter concentrations has been mainly unsatisfactory due to the inability of the electrodes employed to separate the potentials of these species sufficiently to allow for accurate detection.

In addition, neurodegeneration of DA-containing neurons contributes to late-onset neurological diseases, including Parkinson's and Alzheimer's diseases and possibly to normal ageing of the brain [16]. Besides numerous reports have shown their coexistence in biological systems and that they influence each other in their respective activities [17-20]. In the neurotransmission process, DA acts as an extrasynaptic messenger molecule via volume transmission across the synaptic cleft to bind to extra synaptic receptors (G protein-coupled receptors) and transporters [21-23]. However, DA is a unique neurotransmitter as it possesses both excitatory and inhibitory classification. Its vital function lies in regulating attention, cognition, pleasure, movement, and hormonal processes [24,25]. It is widely distributed in the central nervous, renal, hormonal, and cardiovascular systems [26]. Through this, achieving a suitable modification to obtain high sensitivity and selectivity towards DA sensors is the ultimate goal.

Nanomaterial-modified electrodes have many advantages over the traditional material-modified electrodes. Firstly, nanomaterials offer huge specific surface area for the immobilization of functional molecules on the electrodes. Secondly, some semiconductor nanomaterials may act as promoters of electrochemical communications, accelerating the electron transfer rate between proteins and electrodes. Thirdly, some biocompatible nanomaterials can help proteins or cells maintain their activities on the electrode for a long period. Therefore, a variety of nanomaterials have been synthesized and characterized for the performance of electrochemical analysis for proteins and cells. The frequently used nanomaterials include metal nanomaterials, especially nickel nanoparticles (NiNPs).

EXPERIMENTAL

Materials

All chemicals (up to 99.99% purity) were purchased from Sigma Aldrich. The HPLC grade tetra alkyl ammonium bromide salt TOAB and tetrahydrofuran (THF), acetonitrile (ACN) were purchased from Sigma Aldrich and Rankem chemicals and used as such. The sacrificial anode in the form of nickel sheet and platinum sheet as inert cathode having thickness 0.25 mm and purity 99.99% were purchased from Alfa Aesar.

Preparation of Ni NPs modified electrode

2 mg of the Ni NPs were added to 2 mL of 0.1 % nafion alcoholic solution and then sonicated for about 15 min with an ultrasonicator to get a stable and homogenous suspension. To prepare the Au modified electrodes with Ni-AuE nanoparticles, an alcoholic solution of 0.1 % Nafion dispersion of Ni-AuE (1 mg mL^{-1}) was prepared and the suspension ($5\mu\text{L}$) was cast on to the surface of pretreated AuE electrodes. The solvent was allowed to evaporate at room temperature for 2-3 hrs which resulted into immobilized Ni NPs on the Au electrode surface. The modified Ni-AuE electrode was then taken out and washed several times with double distilled water and kept in air. A uniform black film was found to be formed on the AuE surface.

Method

Nickel oxide nanoparticles synthesized by electrochemical method. This method was developed by Reetz in the 1990 [27-28]. The process makes the use of an inexpensive two electrode set up for 25-30 ml electrolyte solution. Including both oxidation of bulk metal and reduction of metal ions for size selective preparation of tetra alkyl ammonium salt stabilized metal nanoparticles. In the initial experiment we have used a nickel metal sheet (1x1 cm) as anode and a platinum sheet (1x1 cm) as the cathode. These two electrodes were placed parallel to one another and were separated by 1cm in 0.01 M solutions of tetra alkyl ammonium salt (TOAB) were prepared in ACN/THF (4:1) served as the supporting electrolyte. The electrolysis process was then carried out by applying current of 10mA/cm^2 for 2 hrs. These nanoparticles after electrolysis were allowed to settle for one day. The agglomerated solid sample was separated from the solution by decantation and washed three to four times with THF. The washed samples were then dried under vacuum in desiccators and calcinated at 400°C and used for characterizations.

CHARACTERIZATION TECHNIQUES

Structural studies of the synthesized nanoparticles was done. The synthesized solid nanoparticles were mixed with KBr and FTIR spectra were recorded in the range of 400 to 4000 cm^{-1} on Jasco FTIR

8400 Spectrophotometer. In UV visible spectroscopic analysis supernatant of synthesized nanoparticles were used to record colour and study surface plasmon absorption in the UV-visible region using Jasco UV-Visible Spectroscopy. The powdered X-ray diffraction patterns were obtained out on X-ray powder diffractometer PW-1840, using CuK α radiation ($\lambda = 1.54 \text{ \AA}$). The samples were scanned from 20-820 at the scan rate of 5×10^4 CPS. The scanning electron microscopy study was carried out on JEOL make JSM 63608A microscope to study the morphology of the synthesized nanoparticles.

Transmission Electron Microscopy of synthesized nanoclusters were ultrasonicated in ethanol and then a drop of the dispersed nanoparticles was placed onto a carbon coated 400 mesh copper grid with format coating over it, followed by natural evaporation. Transmission electron microscopic study and electron diffraction were carried out on Philips CM 200kv.

Cyclic voltammetry (CV) measurements were performed on a Metrohm Autolab PGSTAT128N (Metrohm B.V., Utrecht, Netherlands). One compartment with three electrode system consists of a saturated Ag/AgCl reference electrode, a platinum wire auxiliary electrode and a modified gold electrode as working electrode. Dopamine measurement was carried out in 0.1 PBS solution at RT.

RESULT AND DISCUSSION

UV visible spectroscopic analysis

The reduction of nickel ions was visibly evident from the color changes associated with it. These NiNPs are encapsulated with TOAB which is completely removed only after calcinations. The increase in the intensity of the UV band and shifting to higher wavelength may be due to presence of capping agent. As the electrochemical process is a function of current density, the formation of nanoparticles is diffusion controlled and it also depends on the concentration of ions at the electrode surface and in the bulk. The metal nanoparticles exhibit absorption bands or broad regions of absorption in the UV-Vis range due to the excitation of surface Plasmon resonance (SPR) or interband transitions; these SPR are characteristic properties for the metallic nature of particles. The prominent peak observed at 362 nm in the visible wavelength is due to the absorption of surface Plasmon. A broad peak around 362 nm can be attributed to wide size distribution of particles formed in the solution.

The optical spectra were obtained at current density 10 mA/cm^2 and shown in **Figure 1**. The optical spectra shows absorption bands in the range 360-370nm which confirms the metallic nature.

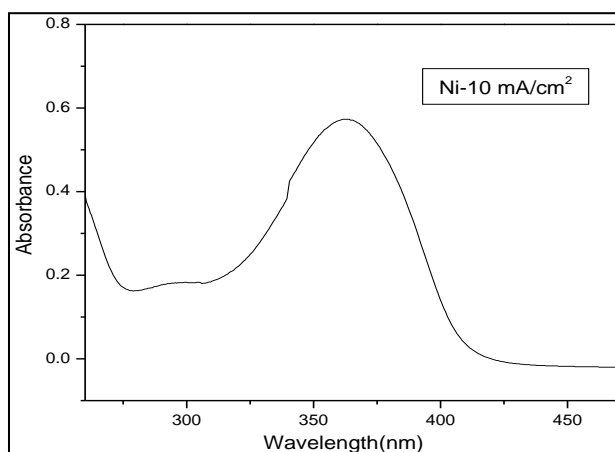


Figure 1: UV-Vis spectrum for nickel nanoparticles capped with TOAB at 10 mA/cm^2 current density

XRD:

The phase confirmation of the as-synthesized NiNPs was carried out using XRD. X-ray line broadening analysis provides a method of finding bulk average size of coherently diffracting domains. X-ray diffraction (XRD) measurements were performed on all NiNPs samples in order to verify the expected crystal structure and estimate average grain sizes. The average crystallite size (D) of solid material can be estimated from X-ray line broadening using the Debye-Scherer equation [29].

$$D = \frac{K\lambda}{\beta \cos \theta}$$

Where, D =Average particle size,

λ = wavelength, θ =diffraction angles, β = FWHM (Full width half maximum)

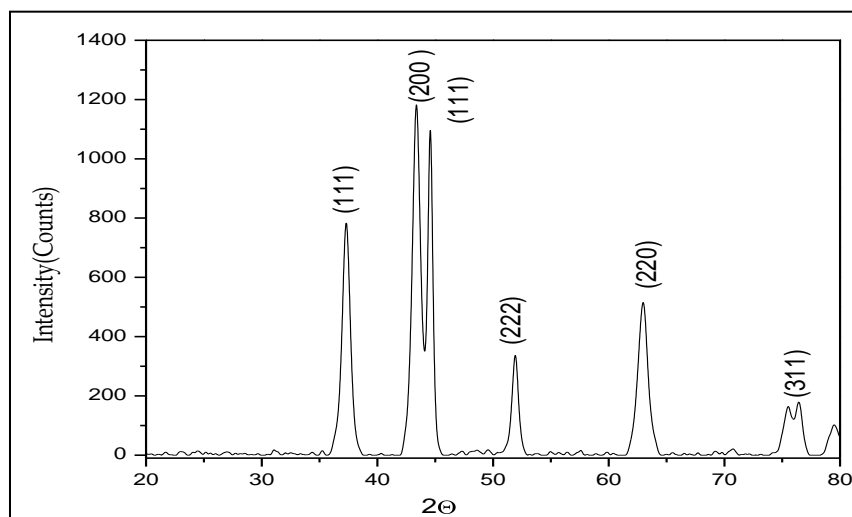


Figure 2: Shows X-ray diffraction pattern of prepared NiO nanoparticles TOAB at 10mA/cm.²

X-ray diffraction (XRD) pattern of the prepared compound reveals the crystalline nature, phase purity and structure details. **Figure 2.** shows the powder XRD pattern recorded for as prepared nickel oxide. The powder X-ray diffraction (XRD) with nickel filtered CuK α ($\lambda = 1.5405 \text{ \AA}$) radiation. Five diffraction peaks were observed at (111), (200), (220), (311) and (222).The peak position and their intensity matched with the standard pattern of FCC type NiO with a space group of Fm3m(225) (Joint Committee on Powder Diffraction Standards (JCPDS) file no. 04-0835)[65,66]. The 2θ values for the planes (111), (200), (220), (311) and (222) were found to be 37.57, 44.5°, 51.94° 62.42° and 76.42° respectively.

Field Emission- Scanning Electron Microscopy

The nickel nanoparticles show the presence of porous nanoparticles. **Figure 3.** Shows FE-SEM image of nickel nanoparticles with TOAB at 10mA/cm². The surface morphology of some nanoparticles is in spherical shape some are globular shape and some are in irregular shape. FE-SEM clearly indicated the decrease in particle size with increase in bulkiness capping agent. As the particles size decreases images observes clear shape of nanoparticles. So we can conclude that the prepared NiO particles are in

nanometer range. The appearance of some particles is in spherical shape and some are in bucky ball like shape.

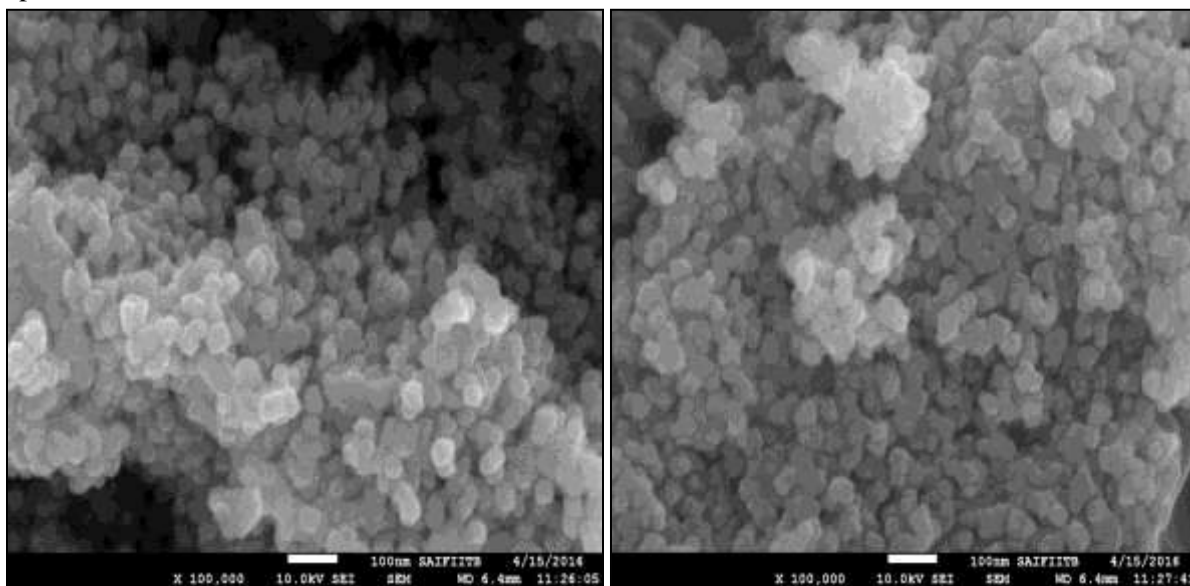
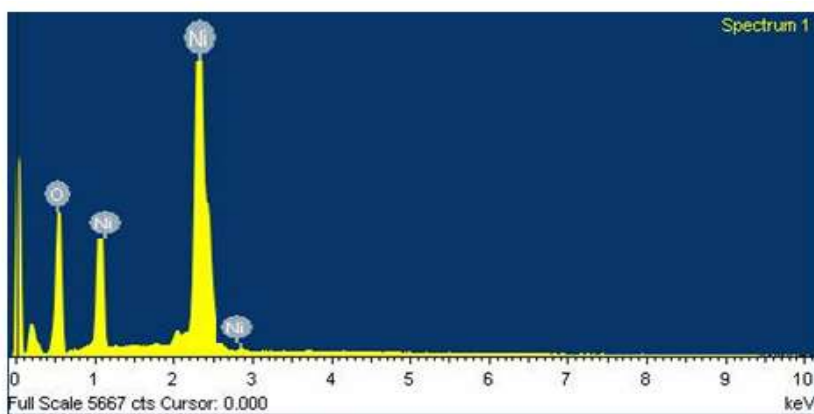


Figure 3: Shows FE-SEM image of nickel nanoparticles with TOAB at 10mA/cm².

EDX

The energy dispersive X-ray analysis (EDX) is performed to know the elemental composition of nickel NPs. Energy-dispersive spectroscopic study confirmed the presence of nickel oxide. The component oxygen showed in the graph is due to the capping agent attributed to partial oxidation of the nanoparticles during the handling of the sample due to atmospheric oxygen. **Figure 4a,b** shows the composition of atomic % of nickel and oxygen which was found to be 90.98 and 9.02 % respectively which clearly shows that formation of pure nickel oxide nanoparticles.

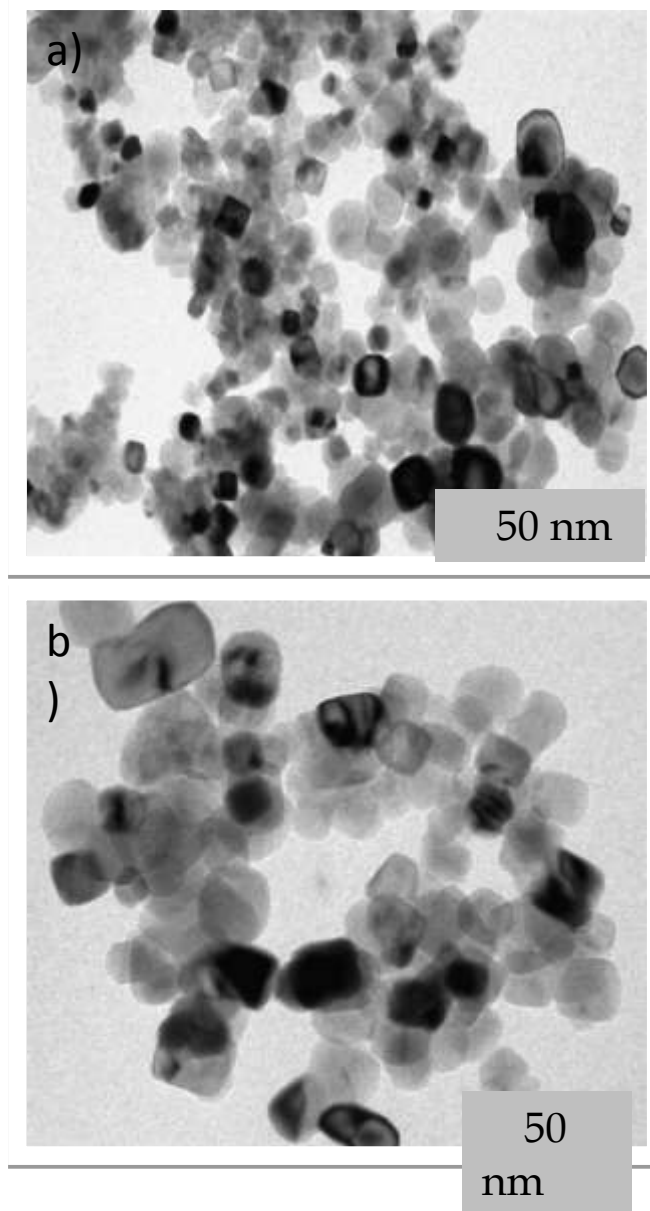


Constituents	Mass (%)	Atom (%)
Ni	97.05	89.96
O	2.95	10.04
Total	100.00	100.00

Figure 4: (a) EDX spectrum of nickel nanoparticles and (b) composition of elements.

TEM

The TEM images depicted in **Figure 5.a** are direct morphological observations of nickel NPs micrographs indicate that most particles were fine with various sizes, spherical, cubic and some clusters have also been observed in the **Figure 5.b**. TEM image along with histogram of particle size distribution of the typical product showed that nickel nanoparticles were dispersed and no aggregation was observed. The average particles size was measured to be 20-40 nm for 10mA/cm² current density, which was in good agreement with calculated particles size by XRD analysis. This indicates that grain growth is affected by the reaction time and is favored three dimensionally (i.e. Cubic formation).



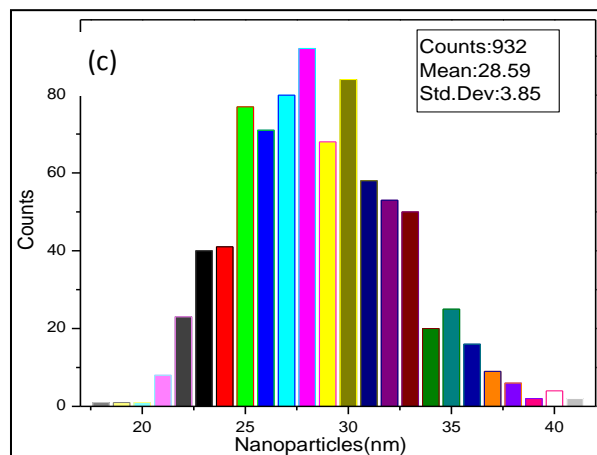


Figure 5-a) & b) TEM images of nickel nanoparticles **c)** particle size histogram of nanoparticles synthesized at current density $10\text{mA}/\text{cm}^2$.

Selected Area Electron Diffraction (SAED) pattern

This could be because the resultant particles were purely metallic nickel with an FCC structure. Electron diffraction was also collected to determine phases of nickel nanoparticles. The electron diffraction pattern of the selected area of nanoparticles shown in **Figure 6** verifies the formation of FCC nickel oxide, for which five ring patterns with plane (111), (200), (220), (311) and (222) of NiO were identified.

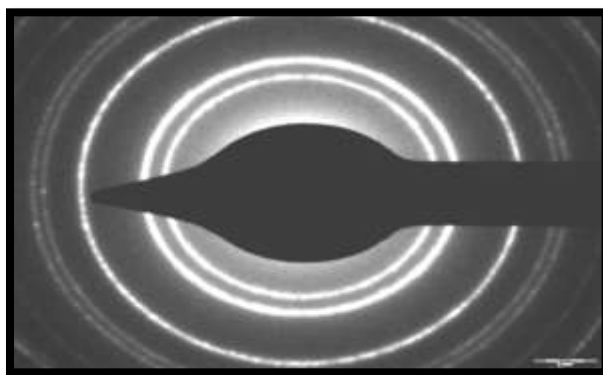


Figure 6: SAED image of the NiO nanoparticles.

Electrochemical analysis

The electrochemical behavior of bare AuE and Ni-AuE were studied by cyclic voltammetry in 0.1 mM ferricyanide at the scan rate 100 mV/s. The cyclic voltammograms depict that modified Ni-AuE showed higher currents in 0.1 mM ferricyanide compared to bare AuE. The increased peak currents are largely the result of increased electro active surface area of modified Ni-AuE. Using diffusion coefficient $6.8 \times 10^{-6} \text{cm}^2/\text{s}$ [30], the cyclic voltammograms on the Ni NPs in the absence and presence of dopamine with different concentrations are shown in **Figure 7a**. and in Randles Sevcik equation, it was seen that the electroactive surface area for modified Ni-AuE was found to be 2.01 times higher than that of bare electrode **Figure 7a**.

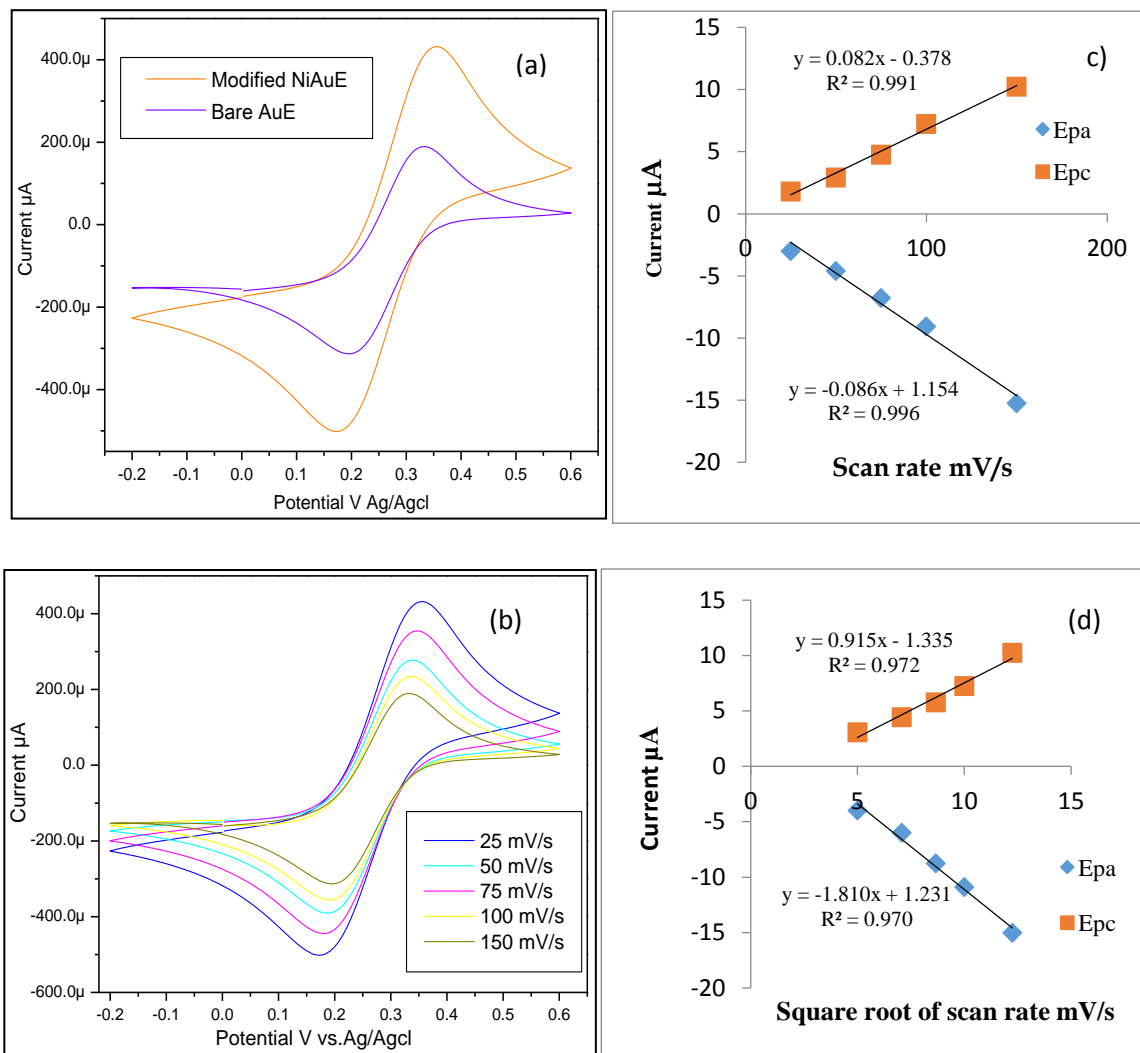


Figure 7 a) CV of bare AuE (voilet) and modified Ni-AuE (orange) b) Cyclic voltammety response of Ni-AuE at different scan rate in 0.1 mM K₃FeCN₆ in 0.1 KNO₃ solution at scan rate from 25,50,75,100, 150 mV/s. Influence of the potential scan rate on the electrochemical response of 0.1 mM K₃FeCN₆ in 0.1 KNO₃ at Ni-AuE. The plot of peak current versus scan rate (c) and the square root of scan rate.

The effect of scan rate on the oxidation and reduction current on Ni-AuE was investigated by cyclic voltammety in 0.1 mM ferricyanide at scan rate in 25-150 mV/s in the potential range -0.2V to 0.6V depicted in **Figure 7b**. The anodic and cathodic peak potential varied linearly with logarithm of scan rate, **Figure 7c** while the oxidation and reduction peak currents linearly increased with the square root of scan rate, **Figure 7d**. This further confirmed that Ni-AuE show reversible behavior in known reversible redox systems such as ferricyanide system.

Electrochemical detection of dopamine by cyclic voltammetr

Effect of varying scan rate:

In order to better understand the electrocatalytic properties of the Ni-AuE for dopamine oxidation, cyclic voltammetric measurements of scan rates were carried out. To investigate the electrocatalytic activity of

Ni- modified AuE in 0.1 PBS solution of 7.4 pH, the CV results of the Ni-AuE were studied in presence and absence of constant concentration 500 μ M dopamine in 0.1 PBS solution at 7.4 pH at scan rate 100mV/s in potential range 0.8V to -0.1V. The recorded CV of 500 μ M dopamine in 0.1 PBS is presented in **Figure 8a**. The characteristics changed significantly during the positive scan two peaks appeared using the modified Ni-AuE. The first peak at 0.50 V was due to the electrochemical adsorption of dopamine, the second peak appearing at 0.102 V was result of electrosorption dopamine. In this case, we observed a shift in potential with increase in scan rate

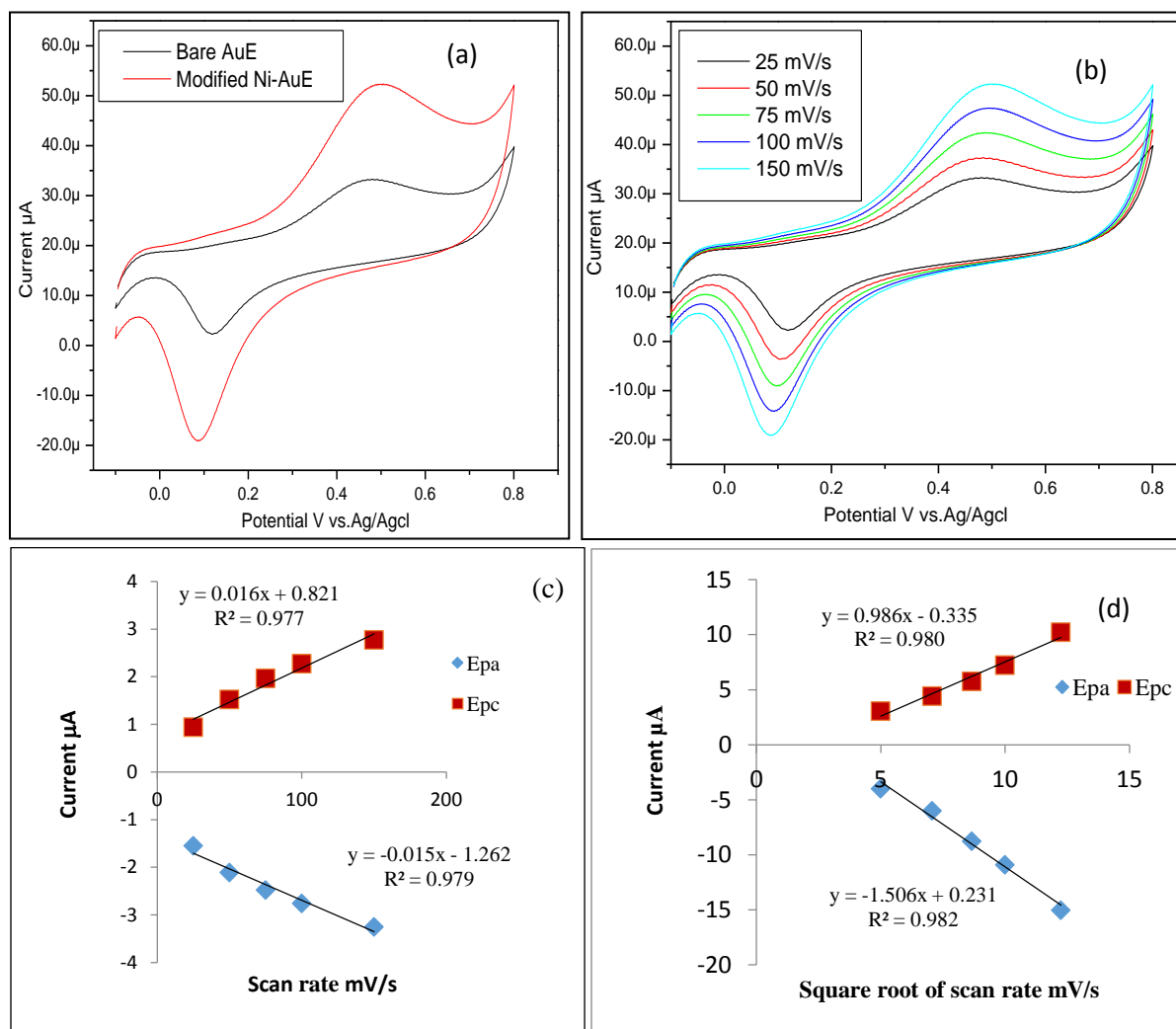


Figure 8 a) CV of bare AuE (black) and Ni-AuE (red) 500 μ M of dopamine b) Response of CV of Ni-AuE at different scan rate from 25,50,75,100, 150 mV/s.. The plot of peak current versus scan rate (c) and d) the square root of scan rate.

The scan rate influence was studied on Ni-AuE using CV at 500 μ M dopamine in 0.1M PBS for scan rate in 25-150 mV/s and potential range -0.1to 0.8 V. From **Figure 8 a**, it can be observed that the peak current increases with increasing scan rate. The anodic peak current were found linear to scan rate with a regression equation of Epa_i (mA) = 0.016x-0.821 and Epc_i (mA) =0.015x+1.261 with correlation coefficient 0.977 and 0.979 respectively **Figure 8c**.The reproducibility of Ni was also investigated by

performing cyclic voltammetric analysis in solution containing 500 μ M dopamine in 0.1M PBS for five different scan rates and the standard deviation 4.28 % which indicate that electrode reproducibly determines the presence of dopamine. The linear relationship of the plot confirmed that the nano particles were electroactive and confined to the surface.

As the scan rate increases, the anodic peak potentials shift to more positive and the cathodic peak potentials convert to negative direction. The peak currents are enhanced with the increasing of the scan rate. According to the plot of the anodic and the cathodic peak currents against the scan rate as shown in **Figure 8d**, it was found that the anodic and the cathodic peak currents are linearly proportional to potential sweep rate, indicating that oxidation of dopamine is surface-controlled in this range of potential scan rate. The sensitivity was found to be 1.000 μ A/ μ M.cm⁻² and 0.6661 μ A/ μ M.cm⁻².

Effect of concentration:

Cyclic voltammetry experiments were carried out with the Ni-AuE to establish the impact of scan rate at different concentration (20-120 μ M) of dopamine in pH 7.0 PBS solutions. In this case, we observed a shift in potential with increase in concentration of dopamine.

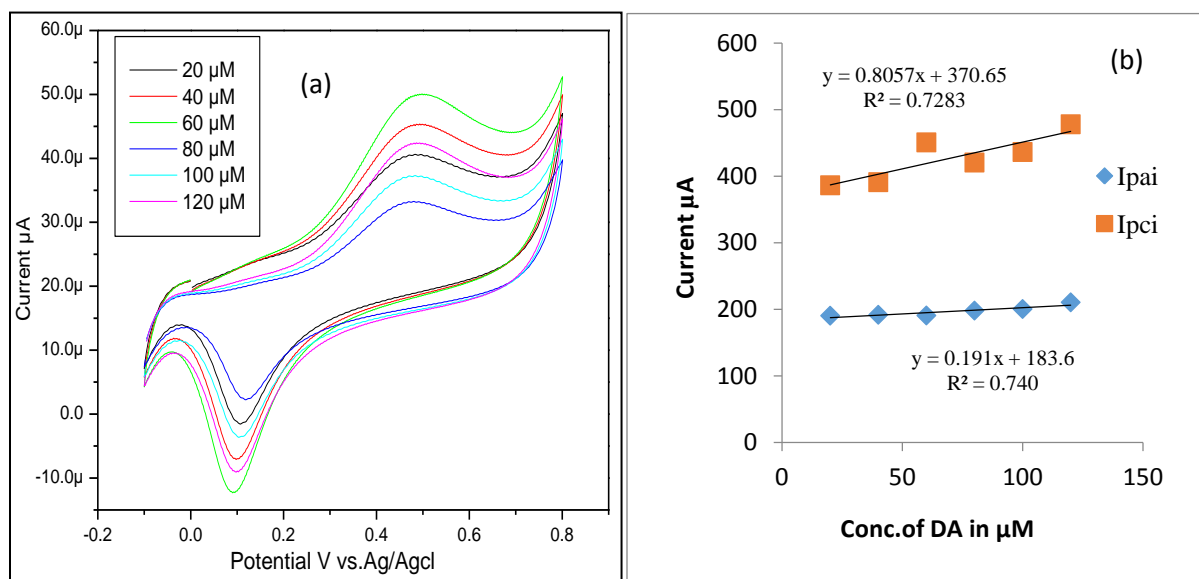


Figure 9 a) Response of CV at Ni-AuE 20 μ M-120 μ M of dopamine in 0.1 PBS of 7.4 pH solution of scan rate 100 mV/s b) The linear plot of peak current I_{pai} and I_{pci} vs. conc. of dopamine

The oxidation peak current was increased with increasing concentration of dopamine. The results **Figure 9b** showed that the peak currents with the potential at around 0.582V were gradually increased by increasing dopamine concentrations. The calibration plot for first and second peak current against the concentration of dopamine was plotted in **Figure 9b** with linear regression equation of with $R^2 = 0.728$ and $R^2 = 0.740$ and the sensitivity was found to be 0.951 μ A/ μ M.cm⁻² and 1.301 μ A/ μ M.cm⁻². The linear relationship of the plot confirmed that the nano particles were electroactive and confined to the surface. This was further confirmed by the plots of peak current against concentration of dopamine. (**Figure 9b**).

Electrochemical detection of dopamine by Differential pulse voltammetry

The determination of DA in the presence Ni-AuE has also been carried out using more sensitive techniques such as differential pulse voltammetry (DPV) technique. **Figure 8a** shows the obtained DPV

impact of Ni-AuE at scan rate i.e. 25-150 mV/s in 0.1M PBS. The result obtained for modified Ni-AuE obtained prominent peak for the absorption of dopamine, the peak appearing at 0.410V. The calibration curve obtained from DPV for peak current against scan rate is plotted in **Figure 8b**. The anodic peak current were found linear to scan rate with a regression equation of $I_{pai}(mA) = 0.590x - 0.730$.

The linear regression equation of with correlation coefficient $R^2 = 0.995$ and the sensitivity was found to be $0.0976 \mu A/\mu M.cm^{-2}$. The linear relationship of the plot confirmed that the nano particles were electroactive. This was further confirmed by the plots of log of peak current against log of scan rate.

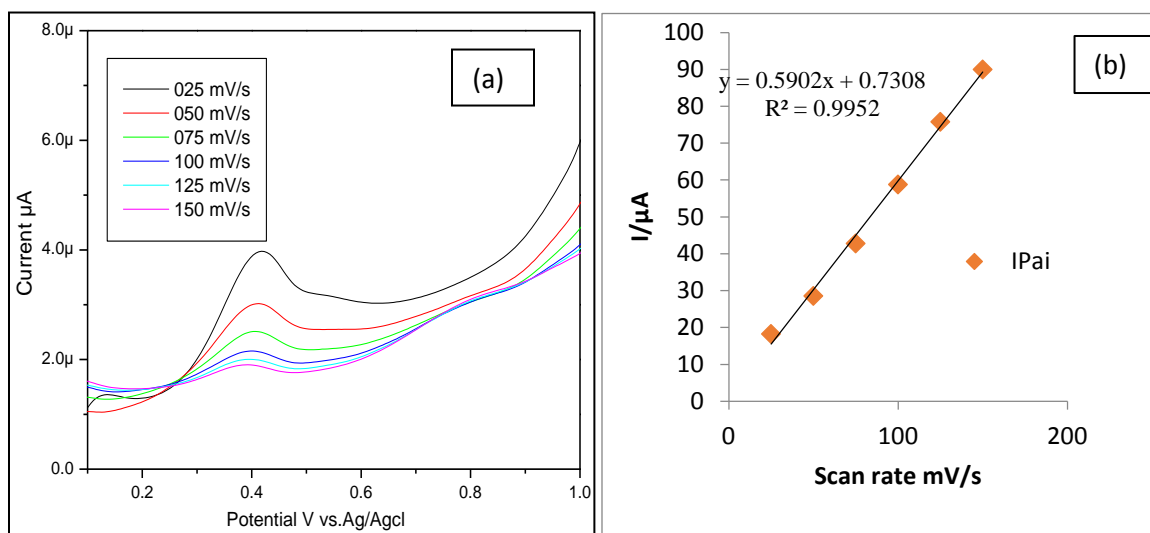


Figure 10 a) Response of DPVs Ni-AuE at 25mV/s-150mV/s of dopamine in 0.1M PBS solution b) linear regression curve for scan rate of dopamine vs. peak current.

CONCLUSION

We have synthesized nickel nanoparticles by electrochemical reduction method. The optical spectra show absorption bands in the range 360-370nm which confirm the metallic nature. The XRD analysis of the nickel nanoparticles showed the formation of Face centered cubic structure. TEM and SEM analysis proved a nearly Cubic morphology of particles. EDX analysis revealed the presence of Ni, O elements indicates that the pure NiO particles are successfully prepared. This work describes the electron transport and electrocatalytic properties of chemically-synthesized NiONPs. It is shown that the Ni-AuE modified electrode gave better electron transport as well as better DA response compared. DA signal were well resolved using DPV techniques compared to CV techniques, with DPV giving the best peak separation of $500\mu M$ at Ni-AuE. Electrocatalysis of DA on the Ni-AuE electrodes was surface-confined electrode process. The study also showed that the NiO modified electrode can be successfully used for the assay of dopamine in DA real life samples.

ACKNOWLEDGEMENTS

The authors are grateful to Department of Chemistry, Dr. Babasaheb Ambedkar Marathwada University, Aurangabad and UGC-SAP-DRS-1 scheme New Delhi for providing laboratory facility. One of the authors (ASR) thankful for financial assistance from Major Research project University Grants Commission, New Delhi. The author (AAA) is also thankful to the University Grants Commission, New Delhi for Rajiv Gandhi National Fellowship.

REFERENCES

- [1] R.N. Adams, "Probing brain chemistry with electroanalytical techniques" (1976) *Anal. Chem.* 48, 1126A-1138A.
- [2] J.R. Cooper, F.E. Bloom, R.H. Roth, "Recent Progress in Hormone Research" (1982) 4th ed. Oxford University Press, New York.
- [3] J. Du, R. Yue, F. Ren, Z. Yao, F. Jiang, P. Yang, Y. Du, Rutin detection using highly electrochemical sensing amplified by an Au–Ag nanoring decorated N-doped graphene nanosheet (2014) *Biosens. Bioelectron.* 53,220–224.
- [4] M. Noroozifar, M. Khorasani-Motlagh, R. Akbari, M.B. Parizi, "Carbon Nanotubes Implanted Manganese-based MOFs for Simultaneous Detection of Biomolecules in Body Fluids" (2011) *Biosens. Bioelectron.* 2, 56–63.
- [5] S.E. Hyman, R.C. Malenka, "Addiction and the brain: the neurobiology of compulsion and its persistence" (2001) *Nat. Rev. Neurosci.* 2, 695–703.
- [6] P.N. Tobler, C.D. Fiorillo, W. Schultz, "Adaptive coding of reward value by dopamine neurons" (2005) *Science* 307, 1642–1645.
- [7] D. Yu, Y. Zeng, Y. Qi, T. Zhou, G. Shi, "A novel electrochemical sensor for determination of dopamine based on AuNPs@SiO₂ core-shell imprinted composite" (2012) *Biosens. Bioelectron.* 38, 270–277.
- [8] D.L. Robinson, A. Hermans, A.T. Seipel, R.M. (2008) *Chem. Rev.* 108, 2554–2584.
- [9] H. Gu, E.L. Varner, S.R. Groskreutz, A.C. Michael, S.G. Weber, "In Vivo Monitoring of Dopamine by Microdialysis with 1 min Temporal Resolution Using Online Capillary Liquid Chromatography with Electrochemical Detection" (2015) *Anal. Chem.* 87,6088–6094.
- [9] Y. Zhou, H. Yan, Q. Xie, S. Huang, J. Liu, Z. Li, S. Yao, "Simultaneous analysis of dopamine and homovanillic acid by high-performance liquid chromatography with wall-jet/thin-layer electrochemical detection" (2013) *Analyst* 138, 7246.
- [10] J.R. Cooper, F.E. Bloom, R.H. Roth, (1982) 4th ed. Oxford University Press, New York.
- [11] J. Du, R. Yue, F. Ren, Z. Yao, F. Jiang, P. Yang, Y. Du, (2014) *Biosens. Bioelectron.* 53,220–224.
- [12] M. Noroozifar, M. Khorasani-Motlagh, R. Akbari, M.B. Parizi, "An electrochemical sensor based on titanium oxide–carbon nanotubes nanocomposite for simultaneous determination of hydroquinone and catechol" (2011) *Biosens. Bioelectron.* 2, 56–63.
- [13] S.E. Hyman, R.C. Malenka, "Addiction and the brain: the neurobiology of compulsion and its persistence" (2001) *Nat. Rev. Neurosci.* 2, 695–703.
- [14] P.N. Tobler, C.D. Fiorillo, W. Schultz, "Adaptive coding of reward value by dopamine neurons" (2005) *Science* 307, 1642–1645.
- [15] D. Yu, Y. Zeng, Y. Qi, T. Zhou, G. Shi, A novel electrochemical sensor for determination of dopamine based on AuNPs@SiO₂ core-shell imprinted composite. (2012) *Biosens. Bioelectron.* 38, 270–277.
- [16] D.L. Robinson, A. Hermans, A.T. Seipel, R.M. "Monitoring Rapid Chemical Communication in the Brain" (2008) *Chem. Rev.* 108, 2554–2584.
- [17] H. Gu, E.L. Varner, S.R. Groskreutz, A.C. Michael, S.G. Weber, "A label-free strategy for measuring the affinity between monoclonal antibody and hapten using microdialysis sampling combined with chemiluminescent detection" (2015) *Anal. Chem.* 87,6088–6094.

- [18] Y. Zhou, H. Yan, Q. Xie, S. Huang, J. Liu, Z. Li, S. Yao, "Determination of guanine and adenine by high-performance liquid chromatography with a self-fabricated wall-jet/thin-layer electrochemical detector at a glassy carbon electrode" (2013) *Analyst* 138, 7246-7253.
- [19] Y. Cheng, J. Wu, C. Guo, X.-G. Li, B. Ding, Y. Li, "A facile water-stable MOF-based "off-on" fluorescent switch for label-free detection of dopamine in biological fluid" (2017) *J. Mater. Chem. B* 5, 2524- 2534.
- [20] A.J. Stewart, J. Hendry, L. Dennany, "Electrochemiluminescent detection of methamphetamine and amphetamine" (2015) *Anal. Chem.* 87, 11847–11853.
- [21] J.J. Feng, H. Guo, Y.F. Li, Y.H. "Single molecular functionalized gold nanoparticles for hydrogen-bonding recognition and colorimetric detection of dopamine with high sensitivity and selectivity" (2013) *ACS Appl. Mater. Interfaces* 5, 1226–1231.
- [22] J.-C. Jin, J.Wu, G.-P. Yang, Y.-L. Wu, Y.-Y. "A microporous anionic metal–organic framework for a highly selective and sensitive electrochemical sensor of Cu²⁺ ions"(2016) *Wang, Chem. Commun.* 52, 8475-8478.
- [23] Y. Zhang, G.M. Zeng, L. Tang, J. Chen, Y. Zhu, X.X. He, Y. He, "Graphene-based Materials in Health and Environment: New Paradigms" (2015) *Anal. Chem.* 87 989–996.
- [24] Y. Dong, L. Yang, L. Zhang, "Simultaneous Electrochemical Detection of Benzimidazole Fungicides Carbendazim and Thiabendazole Using a Novel Nanohybrid Material-Modified Electrode" (2017) *J. Agric. Food Chem.* 65, 727–736.
- [25] H. Rao, M. Chen, H. Ge, Z. Lu, "A novel electrochemical sensor based on Au@PANI composites film modified glassy carbon electrode binding molecular imprinting technique for the determination of melamine"(2017) *Biosens. Bioelectron.* 87,1029–1035.
- [26] Reetz M.T., Helbig W., Quaiser S.A., *Nanosopic Metal Particles – Synthetic Methods and Potential Applications in Active metals* VCH: Weinheim (1996), 279.
- [27] Reetz M.T., Breinbauer R., Wanninger K., *Tetrahedron Lett.*, (1996), 37, 4499.
- [28] Scherrer P., *Göttinger Nachrichten Gesell.*, (1918), 2, 98.
- [29] M.D. Stoller, S.J. Park, Y.W. Zhu, J.H. An, "Ruoff, Graphene-Based Ultracapacitors" (2008) *Nano Lett.* 8 3498-3502.